Molecular Therapy
Nucleic Acids
Original Article

Diverging targets mediate the pathological role of miR-199a-5p and miR-199a-3p by promoting cardiac hypertrophy and fibrosis

Ni Zeng,[1,2,9] Yu-Qing Huang,[3,9] Yu-Min Yan,[4,9] Zhi-Qin Hu,[4] Zhuo Zhang,[5] Jia-Xin Feng,[3] Ji-Shen Guo,[6] Jie-Ning Zhu,[2] Yong-Heng Fu,[1,2] Xi-Pei Wang,[1] Meng-Zhen Zhang,[1,2] Jin-Zhu Duan,[7] Xi-Long Zheng,[8] Jin-Dong Xu,[1] and Zhi-Xin Shan[1,2]

[1]Research Center of Medical Sciences, Guangdong Provincial People's Hospital, Guangdong Academy of Medical Sciences, Guangzhou 510080, China; [2]Guangdong Provincial Key Laboratory of Clinical Pharmacology, Guangdong Cardiovascular Institute, Guangzhou 510080, China; [3]School of Biology and Biological Engineering, South China University of Technology, Guangzhou 510632, China; [4]School of Pharmacy, Southern Medical University, Guangzhou 510515, China; [5]School of Medicine, South China University of Technology, Guangzhou 510632, China; [6]The Second School of Clinical Medicine, Southern Medical University, Guangzhou 510280, China; [7]Institute of Pediatrics, Guangzhou Women and Children's Medical Center, Guangzhou Medical University, Guangzhou, China; [8]Department of Biochemistry & Molecular Biology, Libin Cardiovascular Institute, The University of Calgary, Calgary, Alberta T2N 4N1, Canada

MicroRNA-199a-5p (miR-199a-5p) and -3p are enriched in the myocardium, but it is unknown whether miR-199a-5p and -3p are co-expressed in cardiac remodeling and what roles they have in cardiac hypertrophy and fibrosis. We show that miR-199a-5p and -3p are co-upregulated in the mouse and human myocardium with cardiac remodeling and in Ang-II-treated neonatal mouse ventricular cardiomyocytes (NMVCs) and cardiac fibroblasts (CFs). miR-199a-5p and -3p could aggravate cardiac hypertrophy and fibrosis *in vivo* and *in vitro*. PPAR gamma coactivator 1 alpha (Ppargc1a) and sirtuin 1 (Sirt1) were identified as target genes to mediate miR-199a-5p in promoting both cardiac hypertrophy and fibrosis. However, miR-199a-3p aggravated cardiac hypertrophy and fibrosis through targeting RB transcriptional corepressor 1 (Rb1) and Smad1, respectively. Serum response factor and nuclear factor κB p65 participated in the upregulation of miR-199a-5p and -3p in Ang-II-treated NMVCs and mouse CFs, and could be conversely elevated by miR-199a-5p and -3p. Together, Ppargc1a and Sirt1, Rb1 and Smad1 mediated the pathological effect of miR-199a-5p and -3p by promoting cardiac hypertrophy and fibrosis, respectively. This study suggests a possible new strategy for cardiac remodeling therapy by inhibiting miR-199a-5p and -3p.

INTRODUCTION

Heart failure is typically associated with cardiac remodeling, which is characterized by pathological cardiac hypertrophy and fibrosis. During cardiac hypertrophy and fibrosis, cardiac cells undergo structural changes and become dysfunctional. The histopathological hallmarks of cardiac hypertrophy include myocyte enlargement and myocyte disarray. Cardiac fibrosis is the excessive deposition of extracellular matrix proteins by cardiac fibroblasts (CFs) and myofibroblasts, as well as the disrupted composition of extracellular matrix proteins. Cardiac remodeling occurs in response to a variety of stimuli, including myocardial infarction, mechanical stimulus, cytokines, growth factors, and pressure overload.[1] Since efficient therapeutic approaches are currently unavailable for the management of cardiac remodeling, it is crucial to reveal the molecular mechanisms associated with cardiac hypertrophy and fibrosis and identify new targets to reverse maladaptive cardiac remodeling and even heart failure.

MicroRNAs (miRNAs) are endogenous, 20–23 nucleotide RNAs that negatively regulate target genes involved in various physiological processes and diseases. Accumulating evidence indicates that miRNAs are involved in cardiac remodeling.[2,3] Most miRNA genes are initially transcribed as primary transcripts (pri-miRNAs) by RNA polymerase II (Pol II), which are cleaved to 65–70 nucleotide precursors (pre-miRNAs) by RNA endonuclease Drosha,[4,5] and then cleaved by DICER to produce an miRNA/miRNA* duplex.[4,6] The miRNA/miRNA* duplex is subsequently processed by the RNA-induced silencing complex (RISC) to unwind the duplex at the end with weaker hydrogen binding. The strand with a free 5′ end is selectively included in RISC and served as mature miRNA, while another strand called miRNA* is usually degraded.[4,7] However, both strands can be accumulated *in vivo* if the miRNA/miRNA* duplex does not contain asymmetric hydrogen-binding ends. Moreover, miRNA and miRNA*

Received 10 March 2021; accepted 8 October 2021;
https://doi.org/10.1016/j.omtn.2021.10.013.

[9]These authors contributed equally

Correspondence: Jin-Dong Xu, Research Center of Medical Sciences, Guangdong Provincial People's Hospital, Guangdong Academy of Medical Sciences, Guangzhou, Guangdong Province 510080, P.R. China.
E-mail: xjd8285@163.com
Correspondence: Zhi-Xin Shan, PhD, Research Center of Medical Sciences, Guangdong Provincial People's Hospital, Guangdong Academy of Medical Sciences, Guangzhou, Guangdong Province 510080, P.R. China.
E-mail: shanzhixin@gdph.org.cn

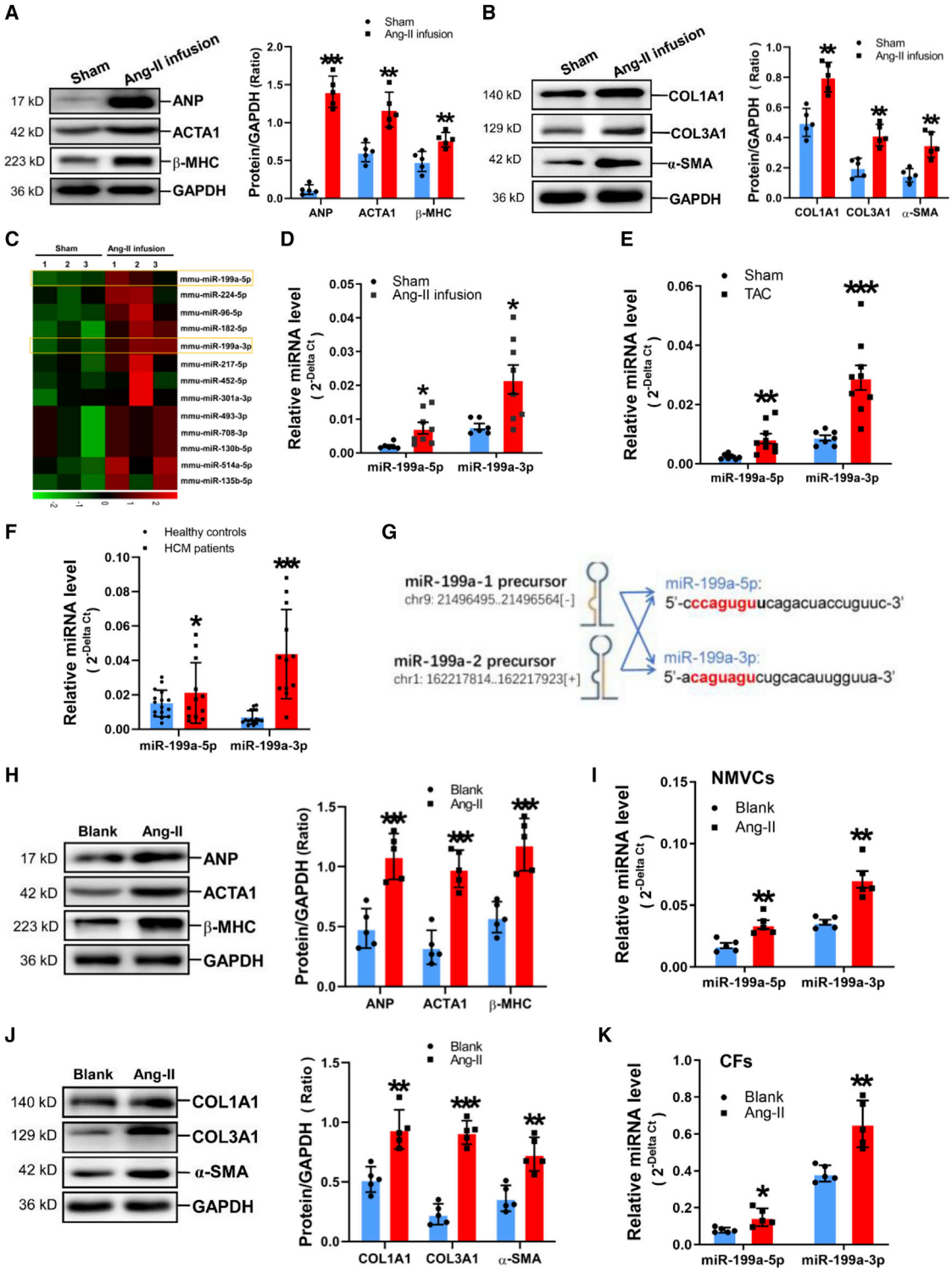

Figure 1. Upregulation of miR-199a-5p and -3p in the myocardium of Ang-II-infused mice and Ang-II-treated NMVCs and mouse CFs

Western blot analysis of ANP, ACTA1, β-MHC (A), COL1A1, COL3A1, and α-SMA (B) in the myocardium of Ang-II-infused mice. (C) Heatmap of miRNA profile showing the dysregulated miRNAs over 1.5-fold in mouse myocardium. (D) qRT-PCR analysis of miR-199a-5p and -3p in the myocardium of Ang-II-infused mice. qRT-PCR analysis of miR-199a-5p and -3p in the myocardium of a mouse model of TAC-induced LV remodeling (E) and in HCM patients (F). (G) MiR-199a-5p and -3p generated

(legend continued on next page)

Table 1. Functional parameters assessed by echocardiography in mice

	Sham+ scramble (n = 8)	Ang-II inf.+ scramble (n = 6)	Ang-II inf.+ miR-199a-5p (n = 8)	Ang-II inf.+ miR-199a-3p (n = 6)
BW (g)	25.2 ± 2.2	23.9 ± 1.8	24.8 ± 2.6	23.3 ± 1.9
Age (weeks)	8	8	8	8
Sex	male	male	male	male
LVPWd (mm)	0.88 ± 0.09	0.72 ± 0.04**	0.69 ± 0.07**	0.75 ± 0.09**
LVPWs (mm)	1.25 ± 0.10	1.10 ± 0.05**	0.97 ± 0.07$^{\#\#}$	0.98 ± 0.09$^{\#}$
LVIDd (mm)	0.90 ± 0.09	0.72 ± 0.04**	0.69 ± 0.07**	0.75 ± 0.09**
LVIDs (mm)	1.32 ± 0.11	1.09 ± 0.10**	0.99 ± 0.13***	1.00 ± 0.13***
Ejection fraction (%)	65.63 ± 5.29	58.10 ± 2.22**	49.81 ± 4.99$^{\#\#}$	49.78 ± 4.06$^{\#\#}$
Fractional shortening (%)	35.14 ± 3.85	29.77 ± 1.46**	24.88 ± 2.87$^{\#\#}$	24.25 ± 2.54$^{\#\#}$

Data are presented as mean ± SD. **p < 0.01, ***p < 0.001 versus sham + scramble, $^{\#}$p < 0.05, $^{\#\#}$p < 0.01 versus Ang-II + scramble by one-way ANOVA with Dunnett's post hoc test. BW, body weight; LVPWd, end-diastolic LV posterior wall diameters; LVPPWs, end-systolic LV posterior wall diameters; LVIDd, end-diastolic LV internal diameters; LVIDs, end-systolic LV internal diameters.

preference always depends on the tissue types, development stages, or disease progression.[8–11] Recent reports showed that frequent co-expression of miRNA-5p and -3p species was observed in induced pluripotent stem cells[12] and colon cancer cells.[13]

MiR-199a-5p[14,15] and miR-199a-3p,[16,17] enriched in heart tissue, can be generated from two different gene loci (www.mirbase.org). To date, it has not been well illustrated whether miR-199a-5p and -3p are co-expressed in cardiac remodeling. Previous studies showed that miR-199a-5p could enhance cardiac hypertrophy,[18,19] but the roles and mechanism of miR-199a-5p in cardiac fibrosis, and miR-199a-3p in cardiac hypertrophy and fibrosis are unrevealed.

In this study, we demonstrated the consistent upregulation of miR-199a-5p and -3p in cardiac hypertrophy and fibrosis and that miR-199a-5p and -3p could enhance cardiac remodeling-related gene expression *in vitro* and *in vivo*. Besides, PPAR gamma coactivator 1 alpha (Ppargc1a) and sirtuin 1 (Sirt-1) were verified as target genes of miR-199a-5p, and Rb-1 and Smad1 were verified as target genes of miR-199a-3p to mediate the pro-cardiac remodeling effects of miR-199a-5p and -3p, respectively. Our results suggested a role for serum response factor (SRF) and nuclear factor κB (NF-κB) p65 in the upregulation of miR-199a-5p and -3p from two miR-199a gene loci during cardiac remodeling. Thus, our study has identified four different novel target genes to mediate the same effects of the congenetic miR-199a-5p and -3p on promoting cardiac hypertrophy and fibrosis.

RESULTS

Co-upregulation of miR-199a-5p and -3p in the hypertrophic and fibrotic mouse myocardium and Ang-II-treated NMVCs and mouse CFs

An animal model of cardiac hypertrophy and fibrosis was established in mice subjected to Ang-II infusion for 4 weeks, demonstrating a significant increase in ANP, ACTA1, β-MHC (Figure 1A), COL1A1, COL3A1, and α-SMA (Figure 1B) in the myocardium. miRNA microarray revealed that the congenetic miR-199a-5p and -3p were upregulated in the myocardium of Ang-II-infused mice (Figure 1C). Results of qRT-PCR assay confirmed that miR-199a-5p and -3p were significantly increased in the myocardium of Ang-II-infused mice (Figure 1D), as well as in the myocardium of a mouse model of transverse aortic constriction (TAC)-induced left ventricular (LV) remodeling (Figure 1E). It was confirmed that miR-199a-5p and -3p were significantly increased in the myocardium of patients with hypertrophic cardiomyopathy (HCM) (Figure 1F).

The DNA templates for miR-199a-1 precursor and miR-199a-2 precursor are shown located in two different genomic loci (http://www.mirbase.org/index.shtml) (Figure 1G). We constructed the recombinant plasmids carrying DNA templates for miR-199a-1 and miR-199a-2 precursors, and confirmed that they could consistently express both miR-199a-5p and -3p in human AC16 cardiomyocytes (Figure S1). We separately isolated the nuclear and cytoplasmic RNA components in AC16 cells for qRT-PCR assay, revealing that miR-199a-5p and -3p were mainly distributed in the cytoplasm of AC16 cells (Figure S2).

Significant increases of ANP, ACTA1, and β-MHC protein were observed in a cell model of Ang-II-induced NMVC hypertrophy (Figure 1H). Results of qRT-PCR verified that miR-199a-5p and -3p were markedly upregulated in Ang-II-treated NMVCs (Figure 1I). Consistently, obvious increases of COL1A1, COL3A1, and α-SMA (Figure 1J), as well as upregulations of miR-199a-5p and -3p (Figure 1K), were shown in a cell model of Ang-II-induced mouse CF fibrosis.

miR-199a-5p and -3p aggravate Ang-II-induced cardiac hypertrophy and fibrosis *in vivo*

Based on a mouse model of Ang-II infusion-induced cardiac hypertrophy and fibrosis, we determined the effects of miR-199a-5p and -3p on the cardiac function and structure after tail vein injection of their mimics. Results of echocardiography showed that the decreases of ejection fraction and fractional shortening, as well as the end-systolic LV posterior wall diameters, were further reduced by injection of miR-199a-5p and -3p mimics, respectively, but not the end-diastolic LV posterior wall diameters and the LV internal diameters (Table 1).

The wheat germ agglutinin (WGA) staining results showed that the cross-sectional size of cardiomyocytes in the myocardium was

from two miR-199a precursors. The seed sequences of miR-199a-5p and -3p are shown in red. Western blot analysis of ANP, ACTA1, and β-MHC (H), and qRT-PCR analysis of miR-199a-5p and -3p (I) in Ang-II-treated NMVCs. Western blot analysis of COL1A1, COL3A1, and α-SMA (J), and qRT-PCR analysis of miR-199a-5p and -3p (K) in Ang-II-treated mouse CFs. All data are presented as mean ± SD. *p < 0.05, **p < 0.01, ***p < 0.001 by unpaired t test. n = 5 (A and B), n = 3 (C), n = 6–8 (D), n = 6–9 (E), n = 12–16 (F), n = 5 (H–K).

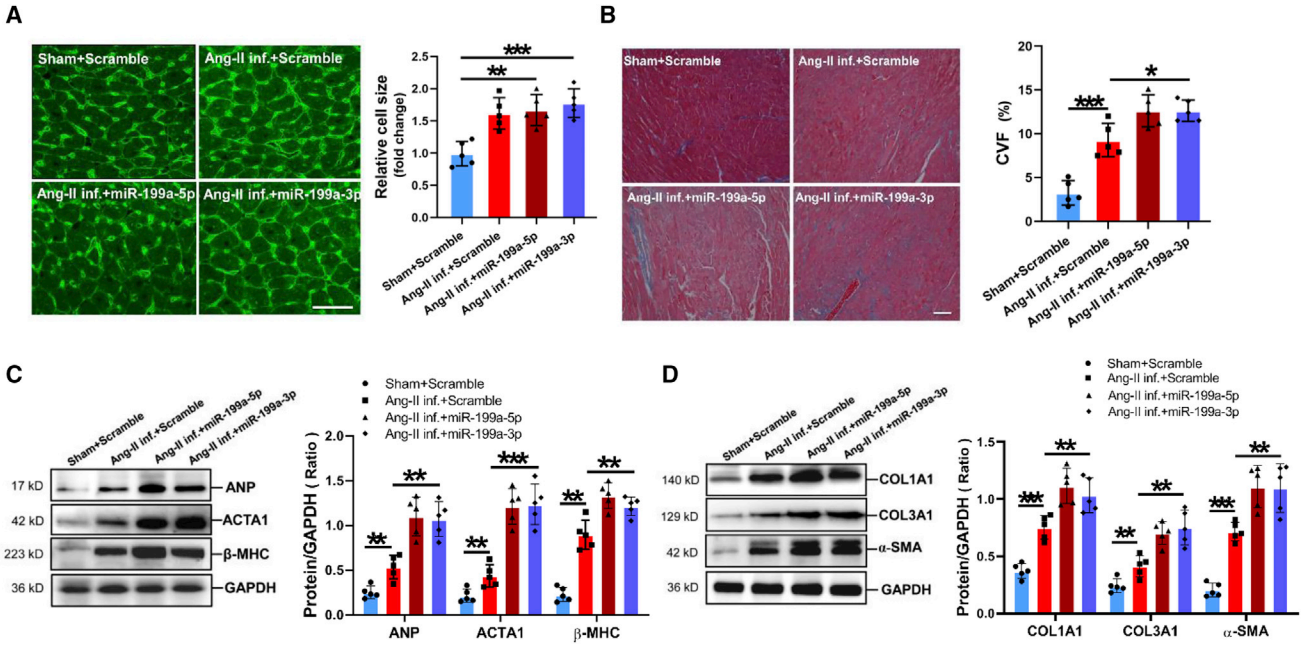

Figure 2. MiR-199a-5p and -3p enhance cardiac hypertrophy and fibrosis in the myocardium of Ang-II-infused mice

WGA staining (A) and Masson's trichrome-staining assay (B) in mouse myocardium. Scale bars, 50 μm in (A) and 100 μm in (B). Western blot analysis of ANP, ACTA1, β-MHC (C), COL1A1, COL3A1, and α-SMA (D) in the myocardium of Ang-II-infused mice received injections of miR-199a-5p and -3p mimics, respectively. All data are presented as mean ± SD. *$p < 0.05$, **$p < 0.01$, ***$p < 0.001$ by one-way ANOVA with Dunnett's post hoc test (n = 5).

consistently increased in Ang-II-infused mice, but no further increase of cross-sectional size of cardiomyocytes was observed by addition of miR-199a-5p or -3p (Figure 2A). However, the results of the Masson's trichrome staining showed that cardiac fibrosis was further increased in Ang-II-infused mice with miR-199a-5p and -3p mimic injection, respectively (Figure 2B).

Moreover, protein expression of ANP, ACTA1, and β-MHC in mouse myocardium in response to Ang-II infusion was further enhanced by miR-199a-5p and -3p mimic treatment (Figure 2C). Consistently, miR-199a-5p and -3p also markedly aggravated Ang-II-induced COL1A1, COL3A1, and α-SMA protein expression in mouse myocardium (Figure 2D). As expected, the levels of miR-199a-5p and -3p were significantly increased in the myocardium of mice subjected to injection of miR-199a-5p or -3p mimic (Figure S3).

miR-199a-5p and -3p enhance cardiac hypertrophy and fibrosis *in vitro*

miR-199a-5p and -3p mimics were shown efficiently delivered into NMVCs and mouse CFs by using lipofectamine reagent (Figure S4). Results of FITC-phalloidin staining showed that cell size was significantly increased in NMVCs by transfection with miR-199a-5p and -3p mimics, respectively (Figure 3A). Protein expression of ANP, ACTA1, and β-MHC was markedly increased in NMVCs after transfection with miR-199a-5p or -3p mimic (Figure 3B). Consistently, COL1A1, COL3A1, and α-SMA protein expression was also significantly elevated in mouse CFs by transfection with miR-199a-5p and -3p mimics, respectively (Figure 3C).

However, no significant difference was found in mouse CF proliferation, as indicated by CCK8 and EdU assays (Figures S5A and S5B). Meanwhile, flow cytometry-based cell-cycle assay showed that no significant difference in cell-cycle stages was observed in mouse CFs by transfection with miR-199a-5p and -3p mimic, respectively (Figure S5C). Consistently, *trans*-well migration assay demonstrated that miR-199a-5p and -3p did not affect the migration of mouse CFs (Figure S5D).

miR-199a-5p enhances NMVC hypertrophy by targeting Ppargc1a

Analyses of the databases Mirdb (www.mirdb.org) and TargetScan-Vert (www.targetscan.org) indicated that Ppargc1a was a potential target gene of miR-199a-5p. The matching positions for miR-199a-5p within 3′ UTR of Ppargc1a mRNA are shown in Figure 4A. Results of the dual luciferase assay showed that miR-199a-5p mimic could specifically interact with the 3′ UTRs of Ppargc1a mRNA, and mutation of four continuous nucleotides complementary to miR-199a-5p seed sequence could abolish the interaction between miR-199a-5p and the 3′ UTRs of Ppargc1a mRNA (Figure 4A).

A transcript containing the firefly luciferase gene and the 3′ UTRs of Ppargc1a mRNA was expressed, and qRT-PCR analysis of the affinity-purified RNA demonstrated a specific enrichment of the firefly

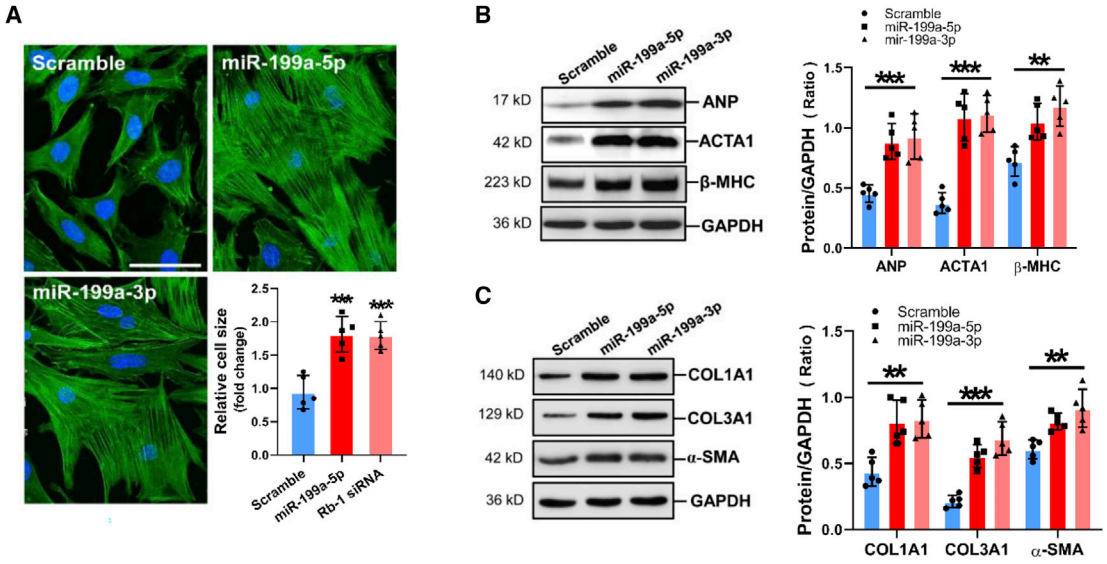

Figure 3. MiR-199a-5p and miR-199a-3p enhance cardiac hypertrophy and fibrosis *in vitro*

(A) Morphology of NMVCs by transfection with miR-199a-5p or -3p as revealed by FITC-phalloidin-staining assay. Scale bar, 50 μm. Western blot analysis of ANP, ACTA1, and β-MHC (B), COL1A1, COL3A1, and α-SMA (C) in NMVCs and mouse CFs by transfection with miR-199a-5p and -3p mimics, respectively. All data are presented as mean ± SD. **p < 0.01, ***p < 0.001 by one-way ANOVA with Dunnett's post hoc test (n = 5).

luciferase gene transcript by miR-199a-5p (Figure 4B). Compared with the scramble-negative control, the protein expression, but not mRNA expression, of Ppargc1a could be significantly inhibited in NMVCs by transfection with miR-199a-5p mimic (Figures 4C and 4D). PGC-1α was also decreased in Ang-II-treated NMVCs and in the myocardium of Ang-II-infused mice, and miR-199a-5p injection further inhibited PGC-1α expression in the myocardium of Ang-II-infused mice (Figures S6A and S6C).

We investigated the effects of miR-199a-5p and Ppargc1a siRNA on cardiomyocyte hypertrophy in NMVCs. The FITC-phalloidin staining showed that the cell size was significantly increased in NMVCs by transfection with miR-199a-5p or Ppargc1a siRNA (Figure 4E). Protein expression of ANP, ACTA1, and β-MHC was also significantly enhanced in NMVCs by transfection with miR-199a-5p and Ppargc1a siRNA, respectively (Figure 4F). Meanwhile, PGC-1α, NRF2, TRX2, SOD2, and HO-1 were found markedly decreased in NMVCs by transfection with either miR-199a-5p or Ppargc1a siRNA (Figure 4F). In addition, adenovirus-mediated overexpression of PGC-1α could efficiently reverse the upregulation of ANP, ACTA1, and β-MHC in miR-199a-5p-treated NMVCs (Figure 4G). Interestingly, we observed that miR-199a-5p and Ppargc1a siRNA could consistently enhance protein expression of fibrosis-related genes, including COL1A1, COL3A1, and α-SMA in mouse CFs (Figure S7A). In addition, adenovirus-mediated overexpression of PGC-1α could efficiently attenuate fibrosis-related gene expression in mouse CFs (Figure S7B).

miR-199a-3p enhances NMVC hypertrophy by targeting Rb-1

Rb-1 was indicated as a target gene of miR-199a-3p by analyzing the databases Mirdb and TargetScan-Vert. The matching positions for miR-199a-3p within the 3′ UTR of Rb-1 mRNA are shown in Figure 5A. Results of the dual luciferase assay indicated that miR-199a-3p mimic could specifically interact with the 3′ UTRs of Rb-1 mRNA (Figure 5A). Expression of the transcript containing the firefly luciferase gene and the 3′ UTRs of Rb-1 mRNA was evaluated, and qRT-PCR analysis of the affinity-purified RNA demonstrated a specific enrichment of the firefly luciferase gene transcript by miR-199a-3p (Figure 5B). Compared with the scramble control, the protein expression, but not mRNA expression, of Rb-1 could be significantly reduced in miR-199a-3p-treated NMVCs (Figures 5C and 5D). It was found that RB-1 was decreased in Ang-II-treated NMVCs and in the myocardium of Ang-II-infused mice, and miR-199a-3p treatment further decreased RB-1 expression in the myocardium of Ang-II-infused mice (Figures S6A and S6C).

We investigated the effects of miR-199a-3p and Rb-1 siRNA on NMVC hypertrophy. The FITC-phalloidin staining showed that the cell size was significantly increased in NMVCs by transfection with miR-199a-3p or Rb-1 siRNA (Figure 5E). Protein expression of ANP, ACTA1, and β-MHC was also significantly increased in NMVCs by transfection with miR-199a-3p and Rb-1 siRNA, respectively (Figure 5F). In addition, western blot results showed that transcription factor E2F2 was decreased in the cytoplasm and increased in the nucleus of NMVCs by transfection with miR-199a-3p mimic or Rb-1 siRNA (Figures 5G and 5H). Moreover, enforced expression of Rb-1 could efficiently inhibit ANP, ACTA1, and β-MHC expression in NMVCs (Figure S8) and reverse the increases of ANP, ACTA1, and β-MHC in miR-199a-5p-treated NMVCs (Figure 5I). However, the effect of knockdown or overexpression of Rb-1 on fibrosis-related gene expression in mouse CFs was not observed in this study (Figures S9A and S9B).

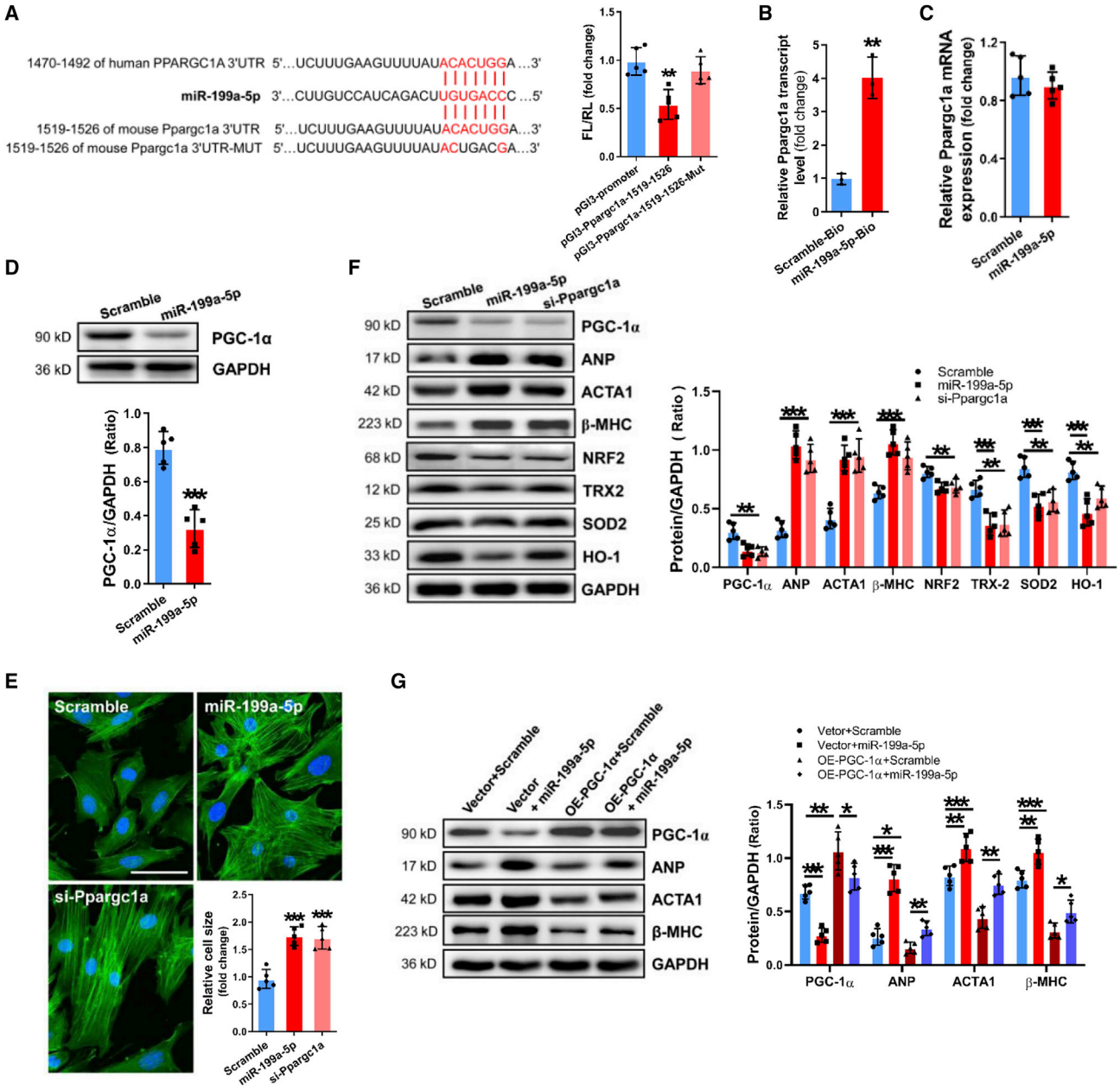

Figure 4. MiR-199a-5p enhances hypertrophy in NMVCs

(A) Verification of Ppargc1a as a target gene of miR-199a-5p by the dual luciferase reporter assay. The seed sequence of miR-199a-5p is CCAGUGU, and the complementary nucleotide sequence to CCAGUGU is shown in red, and the mutated sequence is indicated in bold. (B) RNA pull-down assay to reveal the interaction between miR-199a-5p and the 3′ UTR of Ppargc1a mRNA. qRT-PCR (C) and western blot analysis (D) of Ppargc1a mRNA and protein expression in NMVCs by transfection with miR-199a-5p mimic. (E) Morphology of NMVCs by transfection with miR-199a-5p or Ppargc1a siRNA as revealed by FITC-phalloidin-staining assay. Scale bar, 50 μm. (F) Western blot analysis of PGC-1α, ANP, ACTA1, β-MHC, NRF2, TRX2, SOD2, and HO-1 in NMVCs by transfection with miR-199a-5p and si-Ppargc1a, respectively. (G) Western blot analysis of PGC-1α, ANP, ACTA1, and β-MHC in miR-199a-5p-modified NMVCs with overexpression of PGC-1α. All data are presented as mean ± SD. *$p < 0.05$, **$p < 0.01$, ***$p < 0.001$ by one-way ANOVA with Dunnett's post hoc test in (A, E–G). **$p < 0.01$, ***$p < 0.001$ by unpaired t test in (B–D). n = 5 (A, C–G) and n = 3 (B).

miR-199a-5p enhances mouse CF fibrosis by targeting Sirt1

Sirt1 was predicted as a target gene of miR-199a-5p by analyses of the databases Mirdb and TargetScan-Vert. The matching positions for miR-199a-5p within the 3′ UTR of human and mouse Sirt1 mRNA are shown in Figure 6A. Results of the dual luciferase assay indicated that miR-199a-5p could specifically interact with the 3′ UTRs of Sirt1

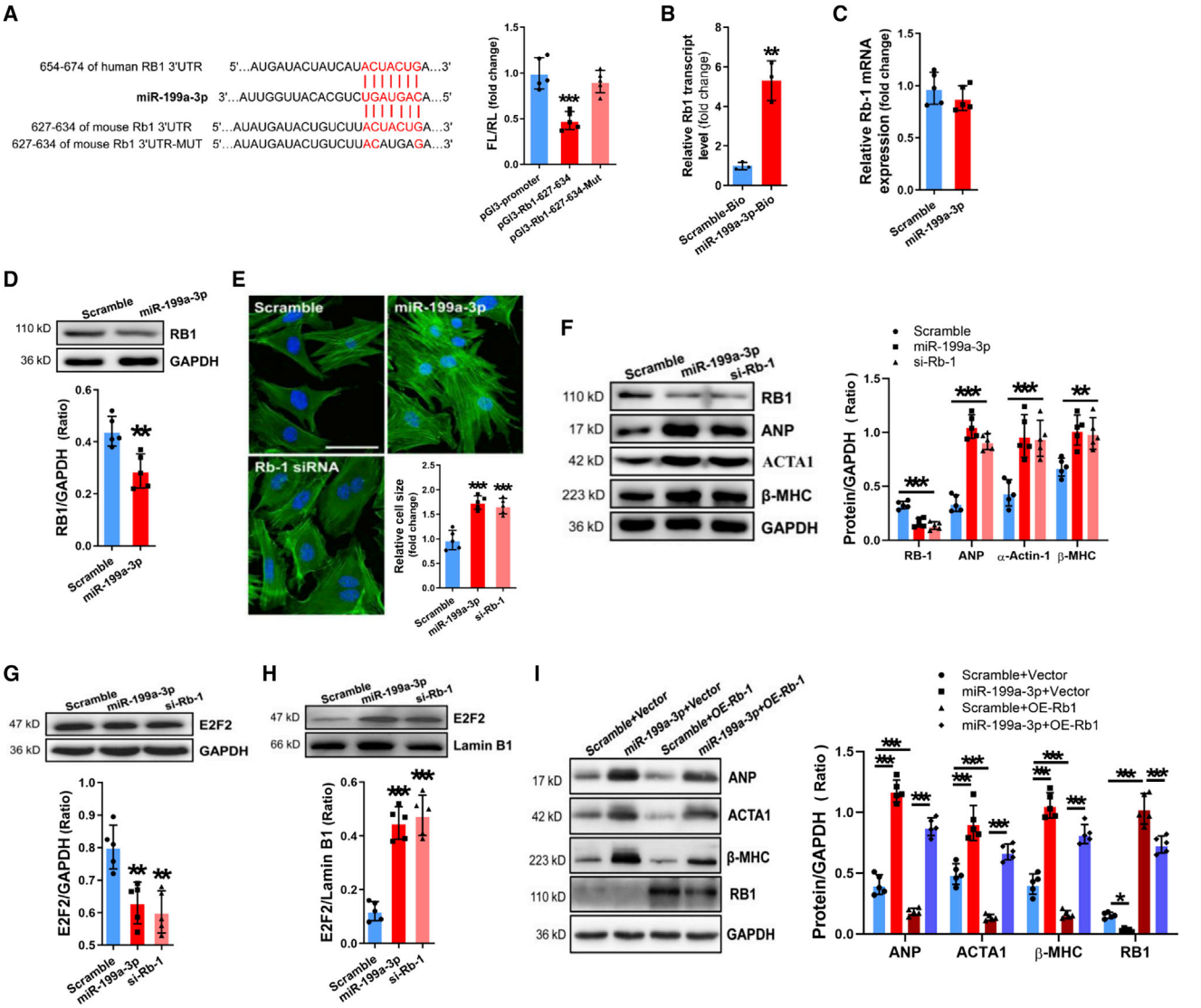

Figure 5. MiR-199a-3p enhances hypertrophy in NMVCs

(A) Verification of Rb1 as a target gene of miR-199a-3p by the dual luciferase reporter assay. The seed sequence of miR-199a-3p is CAGUAGU, and the complementary nucleotide sequence to CAGUAGU is shown in red, and the mutated sequence is shown in bold. (B) RNA pull-down assay to reveal the interaction between miR-199a-3p and the 3′ UTR of Rb1 mRNA. qRT-PCR (C) and western blot analysis (D) of Rb1 mRNA and protein expression in miR-199a-3p-modified NMVCs. (E) Morphology of NMVCs by transfection with miR-199a-3p or Rb1 siRNA as revealed by FITC-phalloidin-staining assay. Scale bar, 50 μm. (F) Western blot analysis of RB1, ANP, ACTA1, and β-MHC in NMVCs by transfection with miR-199a-3p and Rb-1 siRNA, respectively. Western blot analysis of E2F2 protein level in the cytoplasm (G) and nucleus (H) of NMVCs by transfection with miR-199a-3p and Rb-1 siRNA, respectively. (I) Western blot analysis of ANP, ACTA1, β-MHC, and RB1 in miR-199a-3p-modified NMVCs with overexpression of RB1. All data are presented as mean ± SD. *p < 0.05, **p < 0.01, ***p < 0.001 by one-way ANOVA with Dunnett's post hoc test in (A, E–G). **p < 0.01, by unpaired t test in (B–D). n = 5 (A, C–I) and n = 3 (B).

mRNA (Figure 6A). Expression of the transcript containing the firefly luciferase gene transcript and the 3′ UTRs of Sirt1 mRNA was determined, and qRT-PCR analysis of the affinity-purified RNA demonstrated a specific enrichment of the firefly luciferase gene transcript by miR-199a-5p (Figure 6B). Compared with the scramble control, mRNA and protein expression of Sirt1 could be significantly reduced in miR-199a-5p-treated mouse CFs (Figures 6C and 6D). SIRT1 was observed to be decreased in Ang-II-treated mouse CFs and in the myocardium of Ang-II-infused mice, and miR-199a-5p treatment further decreased SIRT1 expression in the myocardium of Ang-II-infused mice (Figures S6B and S6C).

We investigated the effects of miR-199a-5p and Sirt1 siRNA on fibrosis-related genes in mouse CFs. Significant increases of COL1A1, COL3A1,

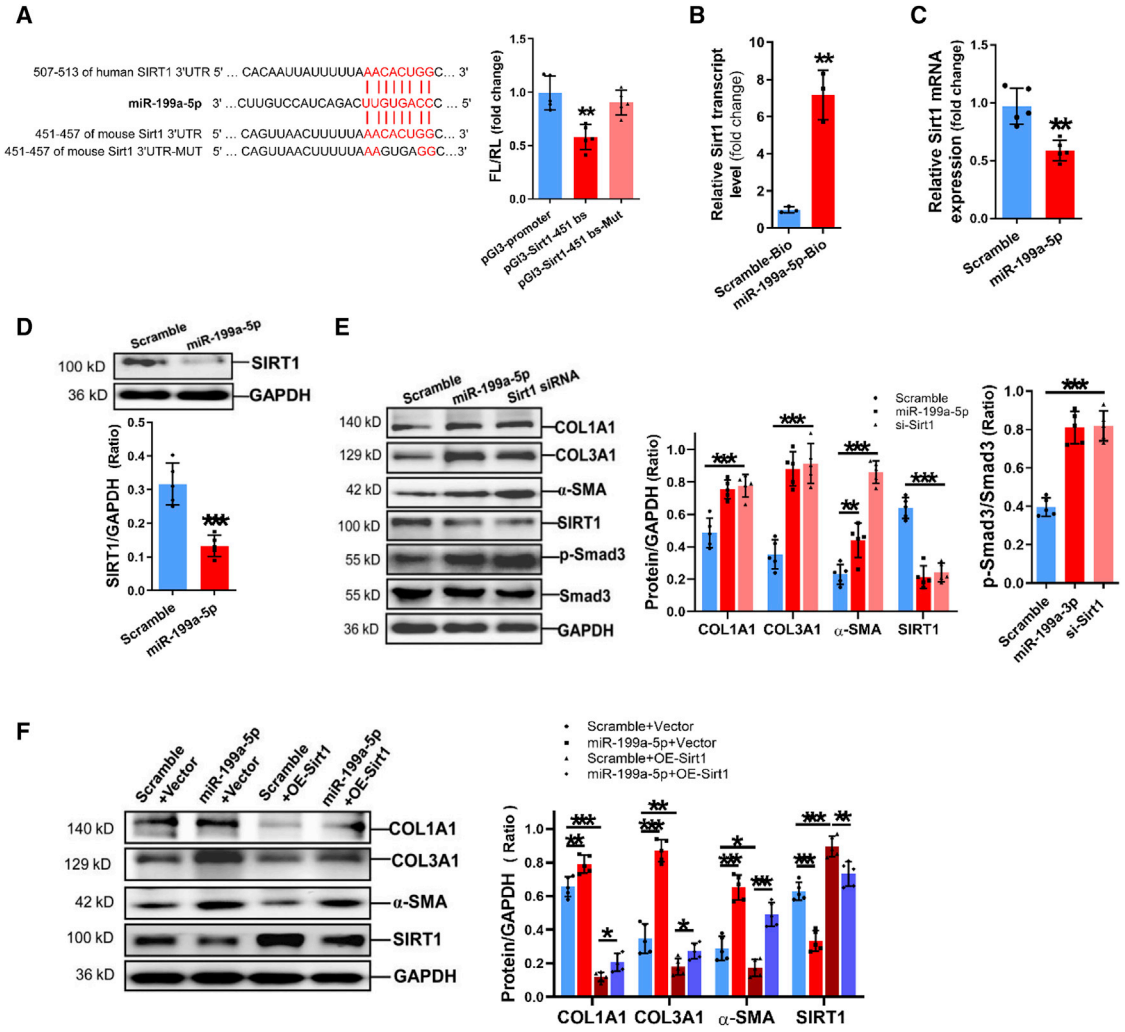

Figure 6. MiR-199a-5p enhances fibrosis-related gene expression in mouse CFs

(A) Verification of Sirt1 as a target gene of miR-199a-5p by the dual luciferase reporter assay. The seed sequence of miR-199a-5p is CCAGUGUU, and the complementary nucleotide sequence to CCAGUGUU is shown in red, and the mutated sequence is indicated in bold. (B) RNA pull-down assay to reveal the interaction between miR-199a-5p and the 3′ UTR of Sirt1 mRNA. qRT-PCR (C) and western blot analysis (D) of Sirt1 mRNA and protein expression in miR-199a-5p-modified mouse CFs. (E) Western blot analysis of COL1A1, COL3A1, α-SMA, SIRT1, and p-Smad3 levels in CFs by transfection with miR-199a-5p and Sirt1 siRNA, respectively. (F) Western blot analysis of COL1A1, COL3A1, α-SMA, and SIRT1 in miR-199a-5p-modified CFs with overexpression of Sirt1. All data are presented as mean ± SD. *$p < 0.05$, **$p < 0.01$, ***$p < 0.001$ by one-way ANOVA with Dunnett's post hoc test in (A, C–F). **$p < 0.01$, ***$p < 0.001$ by unpaired t test in (B–D). n = 5 (A, C–F) and n = 3 (B).

α-SMA expression, and Smad3 activation were observed in mouse CFs in response to transfection with miR-199a-5p or Sirt1 siRNA (Figure 6E). In addition, adenovirus-mediated overexpression of SIRT1 could efficiently reverse the increases of COL1A1, COL3A1, and α-SMA in miR-199a-5p-treated mouse CFs (Figure 6F).

Moreover, we demonstrated that miR-199a-5p and Sirt1 siRNA could efficiently enhance expression of cardiac hypertrophy-related genes, including ANP, ACTA1, and β-MHC in NMVCs (Figure S10A). And overexpression of Sirt1 could markedly attenuate cardiac hypertrophy-related gene expression in NMVCs (Figure S10B).

miR-199a-3p enhances mouse CF fibrosis by targeting Smad1

According to analyses of the databases Mirdb and TargetScan-Vert, Smad1 was predicted as a target gene of miR-199a-3p. The matching positions for miR-199a-5p within the 3′ UTR of human and mouse Smad1 mRNA are shown in Figure 7A. Results of the dual luciferase assay indicated that miR-199a-3p mimic could specifically interact with the 3′ UTRs of Smad1 mRNA (Figure 7A).

Expression of the transcript containing the firefly luciferase gene and the 3′ UTRs of Smad1 mRNA was also determined, and qRT-PCR analysis of the affinity-purified RNA demonstrated a specific enrichment of the

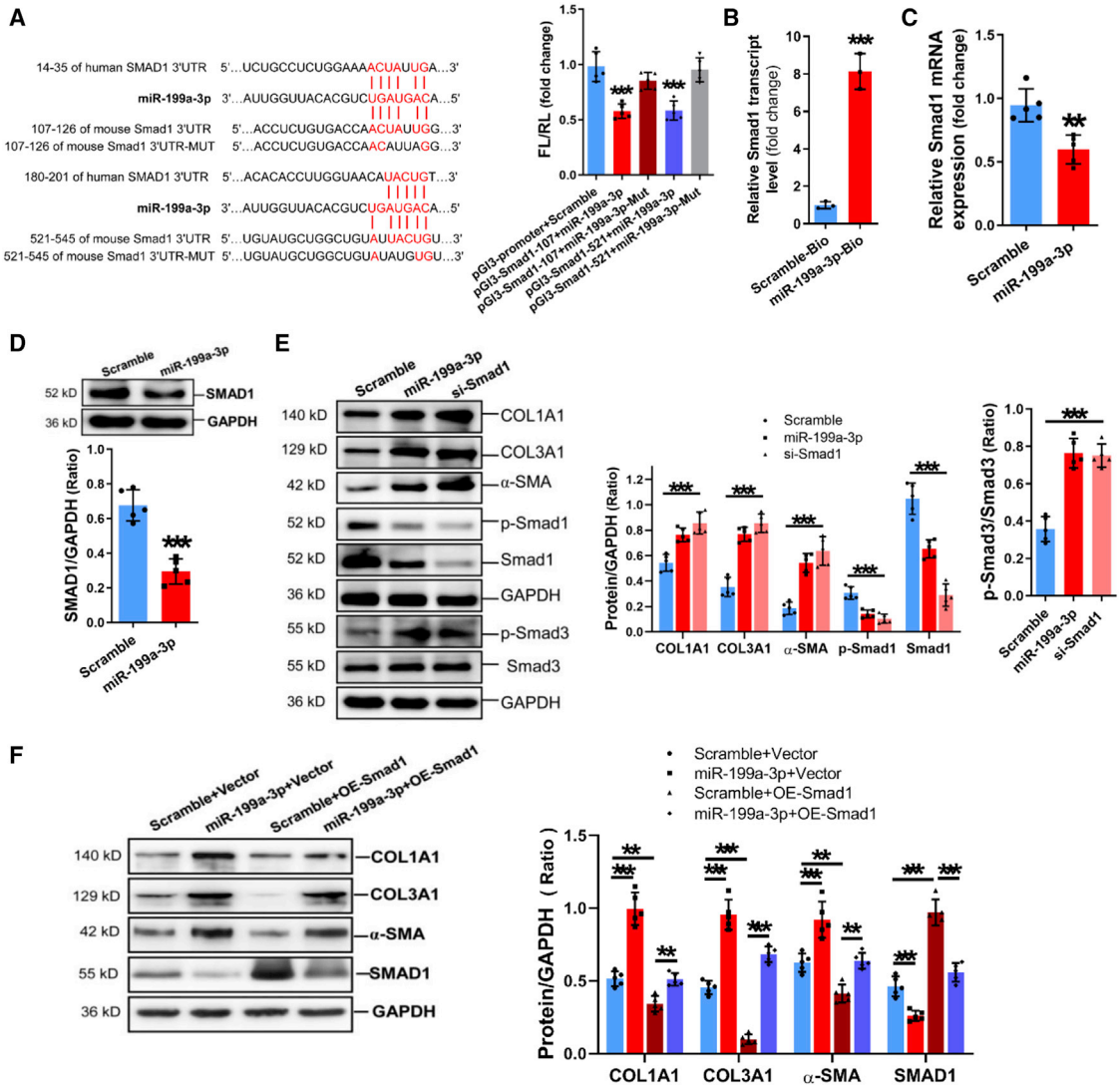

Figure 7. MiR-199a-3p enhances fibrosis-related gene expression in mouse CFs

(A) Verification of Smad1 as a target gene of miR-199a-3p by the dual luciferase reporter assay. The seed sequence of miR-199a-3p is CAGUAGU, and the complementary sequence to CAGUAGU is shown in red, and the mutated sequence is indicated in bold. (B) RNA pull-down assay to reveal the interaction between miR-199a-3p and the 3′ UTR of Smad1 mRNA. qRT-PCR (C) and western blot analysis (D) of Smad1 mRNA and protein expression in mouse CFs by transfection with miR-199a-3p mimic. (E) Western blot analysis of COL1A1, COL3A1, α-SMA, p-Smad1, and p-Smad3 in mouse CFs by transfection with miR-199a-3p and Smad1 siRNA, respectively. (F) Western blot analysis of COL1A1, COL3A1, α-SMA, and SMAD1 in miR-199a-3p-modified CFs with overexpression of Smad1. All data are presented as mean ± SD. **p < 0.01, ***p < 0.001 by one-way ANOVA with Dunnett's post hoc test in (A, C–F). **p < 0.01, ***p < 0.001 by unpaired t test in (B–D). n = 5 (A, C–F) n = 3 (B).

firefly luciferase gene transcript by miR-199a-3p (Figure 7B). Compared with the scramble control, mRNA and protein expression of Smad1 could be significantly inhibited in miR-199a-3p-treated mouse CFs (Figures 7C and 7D). SMAD1 was observed to be decreased in Ang-II-induced CFs and in the myocardium of Ang-II-infused mice, and miR-199a-3p injection further decreased SMAD1 expression in the myocardium of Ang-II-infused mice (Figures S6B and S6C).

Significant decreases of Smad1 and p-Smad1, and obvious Smad3 activation and increases of COL1A1, COL3A1, and α-SMA expression were observed in mouse CFs after transfection with miR-199a-3p and Smad1 siRNA, respectively (Figure 7E). Moreover, adenovirus-mediated overexpression of Smad1 could significantly inhibit COL1A1, COL3A1, and α-SMA expression in CFs (Figure S11). Meanwhile, overexpression of Smad1 could efficiently reverse the increases of COL1A1, COL3A1, and α-SMA expression in miR-199a-3p-treated mouse CFs (Figure 7F). However, the effect of knockdown or overexpression of Smad1 on protein expression of cardiac hypertrophy-related genes in NMVCs was not observed in this study (Figures S12A and S12B).

SRF and NF-κB mediate the upregulation of miR-199a-5p and -3p

Expression of transcription factor SRF was shown to be increased in the myocardium of Ang-II-infused mice and in Ang-II-treated NMVCs (Figures 8A and 8B). To investigate the effect of Ang-II on NF-κB activation, p-NF-κB p65 level was detected in NMVCs at 5, 10, 20, and 60 min after Ang-II treatment. A significant increase of p-NF-κB p65 level was observed in NMVCs at 5, 10, and 20 min in response to Ang-II treatment (Figure 8C). Consistently, a marked increase of NF-κB activation was also found in the myocardium of Ang-II-infused mice (Figure 8A). ChIP-qPCR assays revealed that SRF and NF-κB p65 could specifically bind to the promoter region of miR-199a-1 and miR-199a-2 gene loci in NMVCs (Figures 8D and 8E).

qRT-PCR results showed that upregulations of miR-199a-1 and miR-199a-2 precursors, as well as mature miR-199a-5p and -3p, were observed in Ang-II-treated NMVCs, which could be reversed by Srf siRNA treatment (Figures 8F and 8G).We pre-treated NMVCs with NF-κB p65 inhibitor JSH23 or QNZ for 0.5 h before Ang-II treatment, and found that either JSH23 or QNZ could prevent Ang-II-induced upregulations of miR-199a-1 and miR-199a-2 precursors, as well as mature miR-199a-5p and -3p, in NMVCs (Figures 8H and 8I). Interestingly, we found that miR-199a-5p and -3p could efficiently elevate SRF expression and NF-κB p65 activation in NMVCs (Figure 8J).

Moreover, we observed increased activation of SRF and NF-κB in Ang-II-treated mouse CFs (Figures S13A and S13D), and knockdown of SRF or NF-κB inactivation could also efficiently inhibit Ang-II-induced upregulations of miR-199a-1 and miR-199a-2 precursors (Figures S13B and S13E), as well as mature miR-199a-5p and -3p in mouse CFs (Figures S13C and S13F). Moreover, significant increases of SRF expression and NF-κB p65 activation were also found in mouse CFs by transfection with miR-199a-5p and -3p, respectively (Figure S13G).

DISCUSSION

miR-199a has been shown to participate in the process of cardiac remodeling.[20,21] However, the characteristic expression of miR-199a-5p and -3p in cardiac remodeling was not well illustrated. In this study, we demonstrated the co-upregulation of miR-199a-5p and -3p in the myocardium of HCM patients, as well as in the myocardium of mice subjected to TAC surgery, Ang-II infusion, and ISO injection, respectively. Interestingly, we observed that miR-199a-5p expression was lower than miR-199a-3p in mouse myocardium but higher than miR-199a-3p in human myocardium. These results indicated that the expression pattern of miR-199a-5p and -3p was switched in the myocardium of humans and mice.

Our data showed that miR-199a-5p and -3p could be generated from miR-199a-1 and -2 precursors. Significant increases of SRF and NF-κB p65 were observed in the pathological cardiac remodeling both *in vitro* and *in vivo*, and significant interactions of SRF and NF-κB p65 with the promoter regions of miR-199a-1 and -2 gene loci were shown in NMVCs or mouse CFs exposed to Ang-II treatment. This study demonstrated that SRF and NF-κB p65 mediated the upregulation of miR-199a-1 and -2, as well as miR-199a-5p and -3p, in pathological cardiac remodeling. Interestingly, our data also revealed that miR-199a-5p and -3p could enhance SRF expression and NF-κB p65 activation in NMVCs and mouse CFs, indicating a positive feedback regulation loop between miR-199a-5p/-3p and SRF, and NF-κB p65. However, the mechanism underlying SRF upregulation and NF-κB p65 activation by miR-199a-5p/-3p warrants further investigation.

Our results were supported by a previous report that SRF activated the transcription of miR-199a during myogenic differentiation.[22] However, other studies reported that signal transducer and activator of transcription 3 suppresses miR-199a transcription in mouse cardiomyocytes,[23] and peroxisome proliferator-activated receptor α (PPARα)[24] and PPARγ[25] could activate miR-199a transcription. Therefore, the above data indicated that miR-199a transcription could be modulated by multiple transcription factors and signalings.

miR-199a-5p and -3p can be generated from two different gene loci, miR-199a-1 and miR-199a-2 (www.mirbase.org). The global knockout of miR-199a-2 resulted in embryonic death in mice, but miR-199a-1 knockout failed to achieve the efficient knockdown of miR-199a-5p and -3p in mice (data not shown). To specifically demonstrate the roles of miR-199a-5p and -3p in pathological cardiac remodeling, ago-miR-199a-5p and ago-miR-199a-3p were delivered into Ang-II-infused mice, resulting in aggravated cardiac hypertrophy and fibrosis, and cardiac dysfunction. In addition, miR-199a-5p and -3p mimic could efficiently promote the hypertrophic and fibrotic phenotypes in NMVCs and mouse CFs, respectively. Consistently, previous studies reported that cardiac-specific overexpression of miR-199a-2 or AAV6 vector-mediated expression of the miR-199a-1 pri-miRNA gene, resulting in consistent increases of both miR-199a-5p and -3p, induced cardiac remodeling[18] and sudden arrhythmic death,[26] but knockdown of endogenous miR-199, including both miR-199a-5p and miR-199b-5p, resulted in physiological cardiac hypertrophy.[19]

This study demonstrated that miR-199a-5p and -3p promoted cardiomyocyte hypertrophy via targeting Ppargc1a and Rb-1, respectively. However, Rb-1 was not modulated by miR-199a-5p (Figures S14A and S14B), and Ppargc1a was not modulated by miR-199a-3p in NMVCs (Figures S14C and S14D).

Functionally, we validated that Ppargc1a mediated miR-199a-5p in promoting cardiomyocyte hypertrophy. These data have been supported by a previous report that PGC-1α regulates the expression of the mitochondrial antioxidants against myocardial oxidative stress.[27] We also revealed that transcription factor NRF2 and the downstream antioxidant genes, including TRX2, SOD2, and HO-1, were decreased in NMVCs by transfection with Ppargc1a siRNA and miR-199a-5p, respectively. NRF2, TRX2, SOD2, and HO-1 have been reported to exert myocardial protective effects against cardiac hypertrophy.[28–31] Interestingly, we also showed that Ppargc1a mediated miR-199a-5p in promoting cardiac fibrosis. These results

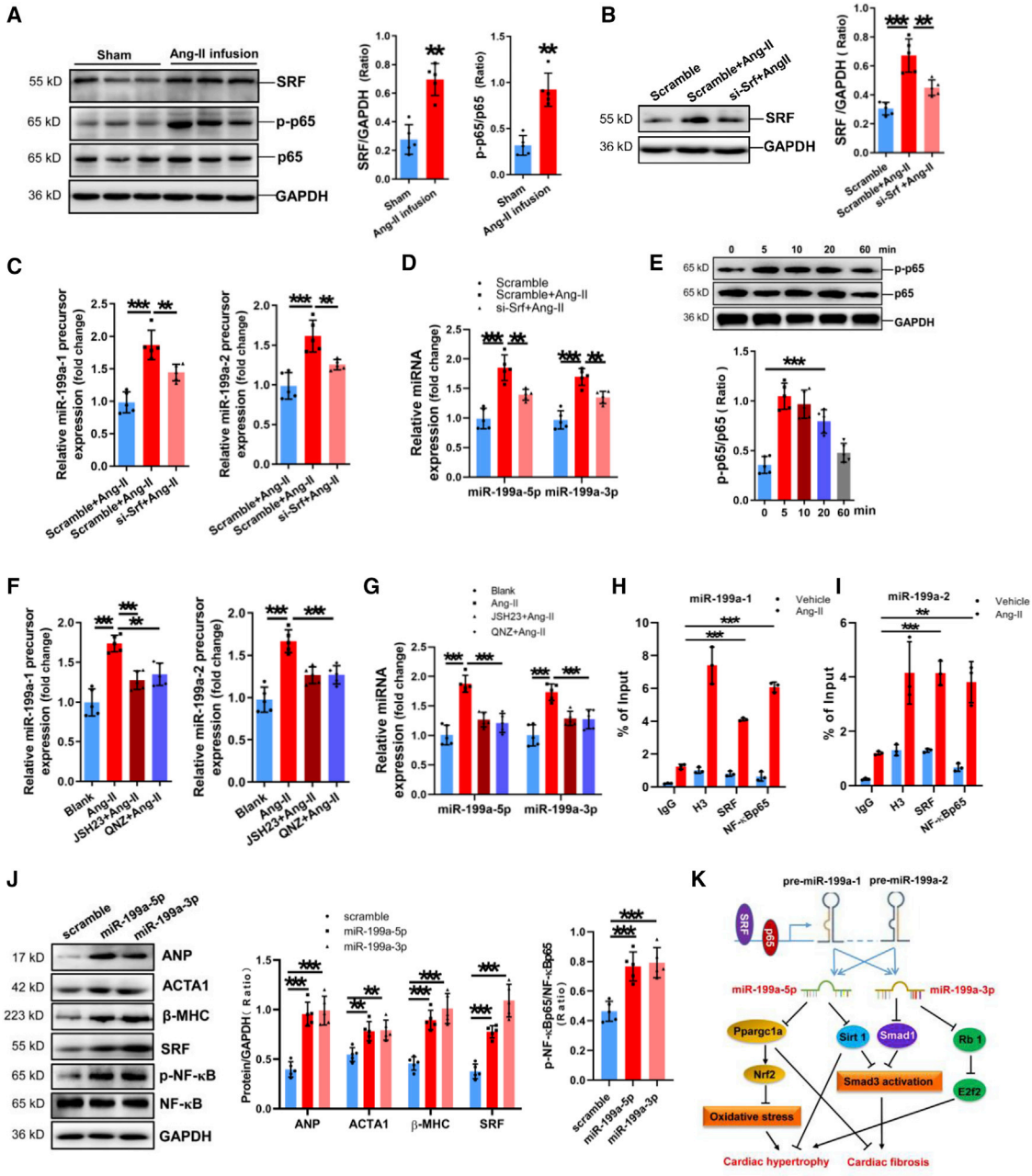

Figure 8. SRF and NF-κB mediate Ang-II- promoted expression of miR-199a-5p and -3p in NMVCs

(A) Western blot analysis of p-NF-κB p65 and SRF levels in the myocardium of Ang-II-infused mice. (B) SRF expression in Ang-II-treated NMVCs with Srf knockdown by western blot assay. Expressions of miR-199a-1 precursor and miR-199a-2 precursor (C) and mature miR-199a-5p and -3p (D) in Ang-II-treated NMVCs with Srf knockdown by qRT-PCR assay. (E) Western blot analysis of NF-κB activation in Ang-II-treated NMVCs. Expressions of miR-199a-1 precursor and miR-199a-2 precursor (F) and mature miR-199a-5p and -3p (G) in Ang-II-treated NMVCs with pretreatment of NF-κB inhibitor, JSH23, and QNZ, by qRT-PCR assay. Chromatin immunoprecipitation-PCR analysis of the binding activities of SRF and NF-κB p65 to the promoter of mouse miR-199a-1 (H) and miR-199a-2 (I) in Ang-II-treated NMVCs. (J) Western blot analysis of hypertrophy-related genes, SRF, and NF-κB p65 activation in NMVCs by transfection with miR-199a-5p and -3p, respectively. (K) Schematic diagram of the mechanism whereby miR-199a-5p and -3p enhances cardiac hypertrophy and fibrosis. All data are presented as mean ± SD. $^{**}p < 0.01$ by unpaired t test in (A, H, and I) $^{**}p < 0.01$, $^{***}p < 0.001$ by one-way ANOVA with Dunnett's post hoc test in (B–G and J). n = 5 (A–G, J) and n = 3 (H and I).

were supported by previous reports that PGC-1α activation alleviated cardiac fibrosis and remodeling.[32–34] We also demonstrated that Rb-1 mediated miR-199a-3p in promoting cardiomyocyte hypertrophy with an increase of nuclear translocation of transcription factor E2F2 in NMVCs. Adult mammalian cardiomyocytes may reenter the cell cycle and cause cardiac hypertrophy,[35,36] and activation of the Rb/E2f signal was reported to participate in cell-cycle progression of cardiomyocytes[37,38] and cardiomyocyte hypertrophy.[39] However, the downstream cardiac hypertrophy-related genes that can be modulated by E2F2 need further investigation.

This study clarified that miR-199a-5p and -3p enhanced cardiac fibrosis through targeting Sirt1 and Smad1, respectively. However, Smad1 could not be modulated by miR-199a-5p (Figures S14E and S14F), and Sirt1 could not be modulated by miR-199a-3p in mouse CFs (Figures S14G and S14H).

In this study, Sirt1 was verified to mediate miR-199a-5p in enhancing Smad3 activation and fibrosis-related gene expression in mouse CFs. Smad3 signal is a principal in cardiac fibrosis,[40,41] and we proved that Sirt1 siRNA and miR-199a-5p could enhance Smad3 activation in mouse CFs, which was consistent with previous reports that Sirt1 could attenuate cardiac fibrosis in a rodent pressure overload model by inhibiting Smad2/3 transactivation,[42] and Sirt1 activation could reduce cardiac fibrosis in a rat model of anthracycline cardiomyopathy.[43] This study also verified that miR-199a-5p could inhibit Sirt1 expression in NMVCs, which was in consistent with the previous report that miR-199a-5p could attenuate Sirt1 expression in cardiomyocytes.[44] Furthermore, our data revealed that Sirt1 also mediated the effect of miR-199a-5p on promoting cardiomyocyte hypertrophy. These results were supported by the previous reports that Sirt1 activation alleviated cardiac hypertrophy and dysfunction.[45–47]

Meanwhile, our data revealed that Smad1 mediated miR-199a-3p in promoting Smad3 activation and fibrosis-related gene expression in in mouse CFs. We clarified that Smad1 was a target gene of miR-199a-3p in mouse CFs, which has been supported by previous reports that Smad1 mediates the function of miR-199a-3p in regulating chondrogenesis[48] and suppressing proliferation and invasion of prostate cancer cells.[49] Currently, very limited information is available on the potential involvement of the Smad1/5/8 cascade in cardiac fibrosis.[50] Our previous study showed that TGFBR3 knockdown could increase fibrosis-related gene expression, along with the Smad1 inactivation and Smad3 activation in human atrial fibroblasts.[51] In this study, we showed that miR-199a-3p could promote fibrosis-related gene expression by suppressing Smad1 activation to increase Smad3 activation in mouse CFs, which has been supported by the previous reports that cardiac fibrosis was associated with Smad1 inactivation and Smad3 activation.[52,53] However, the mechanism underlying the interaction between Smad1 and Smad3 warrants further studies.

Cardiac fibroblast is key player in cardiac fibrosis and responds to myocardial damage by adopting a myofibroblast phenotype and undergoing increased proliferation and migration.[54] Although miR-199a-3p was reported to stimulate rodent cardiomyocyte entry into the cell cycle and cardiac regeneration after myocardial infarction in mice,[55] neither miR-199a-5p nor -3p was observed to affect proliferation and migration of mouse CFs in this study.

In summary, our study demonstrated that miR-199a-5p and -3p were co-upregulated in human and mouse cardiac remodeling, and they could specifically enhance cardiac hypertrophy and fibrosis *in vivo* and *in vitro*. miR-199a-5p promoted cardiac hypertrophy and fibrosis by suppressing both Ppargc1a and Sirt1, however, miR-199a-3p could aggravate cardiac hypertrophy and fibrosis through targeting Rb1 and Smad1, respectively. Furthermore, SRF and activation of the NF-κB signaling pathway participated in the upregulation of miR-199a-5p and -3p in cardiac remodeling; conversely, miR-199a-5p and -3p could positively enhance SRF expression and NF-κB activation in cardiomyocytes and CFs (Figure 8K).

MATERIALS AND METHODS

Ethics statement

The surgically removed LV myocardium was obtained from 12 patients with HCM and 16 healthy organ donors. The clinical investigation was conducted according to the principles expressed in the Declaration of Helsinki and approved by the Research Ethics Committee of Guangdong Provincial People's Hospital (Guangzhou, China) (no. GDREC2019238H(R1)).

Male C57BL/6 mice (24 ± 3 g) were purchased from the Department of Experimental Animal Research Center, Sun Yat-sen University, Guangzhou, China (license no.: SCXK [YUE] 2004-0011). Mice were housed under a 12-h light/dark cycle under pathogen-free conditions and with free access to standard mouse chow and tap water. This study conformed to the Guide for the Care and Use of Laboratory Animals published by the US National Institutes of Health (8th Edition, National Research Council, 2011). The present program was also approved by the Research Ethics Committee of Guangdong Provincial People's Hospital (approval no. GDREC2014066A).

Animal studies

According to our previous report,[56] we established mouse cardiac remodeling models using Ang-II (1.46 mg/kg/day, 28 days) infusion or pressure-overloading by TAC (with eight mice randomized in each group). Meanwhile, 25 nmol ago-miR-199a-5p and ago-miR-199a-3p, i.e., miR-199a-5p and -3p mimic with cholesterol modification, were delivered into a mouse model of Ang-II infusion-induced cardiac remodeling via five times interval tail vein injection, respectively.

Echocardiographic study

Transthoracic echocardiography was performed as reported previously.[56] After the induction of light general anesthesia, the mice underwent transthoracic two-dimensional guided M-mode echocardiography with an 8.5 MHz transducer (Acuson, Mountain View, CA). Echocardiographic measurements were averaged from at least three separate cardiac cycles.

Histological analysis

According to our previous report,[57] the myocardium tissue sections were mounted on regular glass slides and stained with 1.0 mg/mL Alexa Fluor 488 conjugate of WGA solution (Molecular Probes, Eugene, OR, USA) to show the cross-sectional area of cardiomyocytes in mouse ventricular myocardium. Tissue sections were also stained with Masson's trichrome for histological analysis. To analyze the collagen volume fraction (CVF) in mouse ventricular myocardium, we selected eight separate views and assessed the CVF using the formula: CVF = collagen area/total area.

miRNA array

miRNA expression analysis was performed on total RNA extracted from myocardium samples of three Ang-II-infused mice and three sham controls using TRIzol reagent (Invitrogen, Carlsbad, CA, USA). The Agilent/mouse miRNA microarray was used for miRNA expression profiles (Aksomics, Shanghai, China). In brief, 200 ng of total RNA extracted from myocardium samples was fluorescently labeled with cyanine3-pCp using the miRNA Complete Labeling and Hyb Kit (Agilent Technologies, Santa Clara, CA, USA). The labeled samples were then concentrated and hybridized with Hybridization Chamber gasket slides (Agilent Technologies). Arrays were scanned on an Agilent chip scanner (G2565CA), and image analysis was performed using Agilent Feature Extraction (v.10.7) software (Agilent Technologies), followed by data normalization using Agilent Gene Spring software (Agilent Technologies).

Isolation and culture of NMVCs and mouse CFs

NMVCs and CFs were isolated from the hearts of 1- to 3-day-old newborn C57BL/6 mice and cultured as described previously.[56,57] The mouse heart tissue was collected and digested using 0.25% trypsin plus 20 IU/mL DNase. Mouse CFs were separated from cardiomyocytes by gravity separation and grown to confluency on 10-cm cell culture dishes in growth medium (DMEM/F12, 10% FBS, 1% penicillin, and 1% streptomycin) at 37°C in humid air with 5% CO_2.

FITC-phalloidin staining

FITC-phalloidin staining on NMVCs was performed as described previously.[39] The cultured NMVCs were washed in PBS, fixed with 3.7% formaldehyde for 10 min, and permeabilized for 10 min in 0.1% Triton X-100. Monolayers were then washed in blocking solution and incubated for 40 min with FITC-phalloidin (10 μg/mL, Sigma-Aldrich) at 37°C. Monolayers were then washed again, post-fixed with 3.7% formaldehyde, and mounted. Confocal micrographs were obtained using a Leica SP5 confocal microscopy (Leica, Mannheim, Germany). Cell size (total area) was quantified using MiVnt imaging software (Weiyu, Zhuhai, China).

Cell proliferation and migration assays

According to the manufacturer's instructions, EdU staining and CCK8 assays were conducted to determine the proliferation capacity of mouse CFs. *trans*-Well migration assay was performed to assess the migration capacity of mouse CFs. In brief, mouse CFs were cultured in the upper chamber with a higher concentration of fetal bovine serum in the medium in the lower chamber. The number of mouse CFs migrating into the lower chamber was counted to evaluate the migration capacity of mouse CFs.

For cell-cycle analysis, mouse CFs were trypsinized and washed twice with PBS, followed by centrifugation at 500 × *g* for 5 min. CFs pellets were re-suspended in 1 mL nuclear isolation and staining solution (NPE Systems, FL, USA) for 2 min in the dark. DNA content was determined with a Beckman Coulter Quanta SC MPL flow cytometer using the Multicycle software (Beckman, Brea, CA, USA). The results are presented as the percent of the cell population in each cell-cycle phase.

Dual luciferase assay

As our previous report,[58] the recombinant luciferase reporter plasmids containing the potential miR-199a-5p and -3p binding site sequences in the 3′ UTRs of candidate target genes were constructed. Sequence mutations of the potential miR-199a-5p or -3p binding sites in the recombinant plasmids were performed using a site-directed mutagenesis kit (TransGen, Beijing, China) and confirmed by DNA sequencing assay. The luciferase reporter assay was performed using HEK293 cells, and the luciferase activities were determined by the dual luciferase reporter assay system (Promega) according to the manufacturer's protocol.

RNA extraction, RT-PCR, and quantitative real-time PCR

Total RNA was extracted from frozen myocardium tissue, NMVCs, and CFs with TRIzol reagent (Invitrogen), followed by cDNA synthesis and quantitative real-time PCR (qPCR) as described in our previous report.[39] The $2^{-\Delta Ct}$ and $2^{-\Delta\Delta Ct}$ methods were used to calculate relative expression levels of the concerned coding genes and miRNAs, respectively. PCR primers used in this study and the size of fragments amplified are shown in the Table S1.

Identification of miRNA targets based on affinity purification

Identifications of interactions between miR-199a-5p or -3p and their corresponding target gene mRNA were performed as described previously.[59] miR-199a-5p and -3p duplexes were produced carrying a biotin group attached to the 3′ end of the miRNA sense strand. The biotinylated synthetic duplexes and the recombinant plasmids containing firefly luciferase gene in joint with the 3′ UTRs of candidate target genes of miR-199a-5p or -3p were transfected into HEK293 cells for 24 h. Then cell lysis was collected, and miR-199a-5p or -3p target gene 3′ UTR complexes were captured on streptavidin beads from which the corresponding target gene 3′ UTR fragments could be purified and determined. The firefly luciferase gene (*Luci*) transcript was detected to indicate the amount of the captured 3′ UTRs of candidate target genes of miR-199a-5p or -3p.

Western blot assay

Western blot assays were performed as described previously,[39] using anti-ANP, anti-β-MHC, anti-α-SMA, anti-p-Smad1, anti-Smad1, anti-SRF, anti-E2F2, anti-PGC-1α, anti-NRF2 (Abcam), anti-ACTA1,

anti-COL1A1, anti-COL3A1, anti-TRX2, anti-SOD2, anti-HO-1, anti-SRF (Proteintech), anti-SIRT1, anti-p-Smad3, anti-Smad3, anti-p-NF-κB p65, anti-NF-κB p65 (Cell Signaling Technology), anti-RB1or anti-GAPDH (Santa Cruz Biotechnology).

Chromatin immunoprecipitation qPCR

Chromatin immunoprecipitation (ChIP) assay was performed according to the standard crosslinking ChIP protocol (CST technique) with minor modifications.[60] In brief, NMVCs or mouse CFs subjected to Ang-II treatment were harvested and crosslinked with 1% formaldehyde for 10 min at room temperature. After sonication, the soluble chromatin was incubated with 5 μg antibody. Chromatin immunocomplexes were then precipitated with ChIP-Grade Protein G Magnetic Beads (CST, 9006). The immunoprecipitated complex was washed, and DNA was extracted and purified by DNA Purification Buffers and Spin Columns (CST, 14209). ChIP DNA was analyzed by real-time PCR using specific primers, and the data were normalized by input DNA. The antibodies used in this study included anti-SRF and anti-NF-κB p65. PCR primers were shown in the Table S1.

Statistical analysis

Data are presented as the mean ± standard deviation (SD). For analysis of differences between two groups, Student's t test was performed. One-way ANOVA followed by post hoc test (Bonferroni) was chosen for the comparisons of interest without adjustment for multiple comparisons. In all experiments, differences were considered significant when p was less than 0.05. Analyses were performed in IBM SPSS Statistics 25 (IBM Corp, Armonk, NY, USA).

SUPPLEMENTAL INFORMATION

Supplemental information can be found online at https://doi.org/10.1016/j.omtn.2021.10.013.

ACKNOWLEDGMENTS

This work was supported by the following grants: National Science Foundation of China (grant nos. 82070254, 81770264, and 81470439), Guangzhou Science and Technology Program Project (202002030013, 202002030039, and 202102080093), and a High-level Hospital Construction Project of Guangdong Provincial People's Hospital (DFJH201902).

AUTHOR CONTRIBUTIONS

N.Z., Y.-Q.H., Y.-M.Y., J.-X.F., and J.-S.G. performed the functional experiments and analyzed the data. Z.-Q.H. and Z.Z. performed critical bioinformatics analyses. J.-N.Z., Y.-H.F., and X.-P.W. provided technical support and analyzed the data. M.-Z.Z., J.-Z.D., and X.-L.Z. provided academic advice to the study and revised the manuscript. J.-D.X. and Z.-X.S. designed the study, and wrote and revised the manuscript.

DECLARATION OF INTERESTS

The authors declared no competing interests.

REFERENCES

1. Perrino, C., Naga Prasad, S.V., Mao, L., Noma, T., Yan, Z., Kim, H.S., Smithies, O., and Rockman, H.A. (2006). Intermittent pressure overload triggers hypertrophy-independent cardiac dysfunction and vascular rarefaction. J. Clin. Invest. *116*, 1547–1560.
2. Chen, C., Ponnusamy, M., Liu, C., Gao, J., Wang, K., and Li, P. (2017). MicroRNA as a therapeutic target in cardiac remodeling. Biomed. Res. Int. *2017*, 1278436.
3. Li, Y., Liang, Y., Zhu, Y., Zhang, Y., and Bei, Y. (2018). Noncoding RNAs in cardiac hypertrophy. J. Cardiovasc. Transl. Res. *11*, 439–449.
4. Bartel, D.P. (2004). MicroRNAs: genomics, biogenesis, mechanism, and function. Cell *116*, 281–297.
5. Ha, M., and Kim, V.N. (2014). Regulation of microRNA biogenesis. Nat. Rev. Mol. Cell Biol. *15*, 509–524.
6. Bartel, D.P. (2009). MicroRNAs: target recognition and regulatory functions. Cell *136*, 215–233.
7. Schwarz, D.S., Hutvágner, G., Du, T., Xu, Z., Aronin, N., and Zamore, P.D. (2003). Asymmetry in the assembly of the RNAi enzyme complex. Cell *115*, 199–208.
8. Li, S.C., Chan, W.C., Ho, M.R., Tsai, K.W., Hu, L.Y., Lai, C.H., Hsu, C.N., Hwang, P.P., and Lin, W.C. (2010). Discovery and characterization of medaka miRNA genes by next generation sequencing platform. BMC. Genomics *11* (*Suppl 4*), S8.
9. Griffiths-Jones, S., Hui, J.H., Marco, A., and Ronshaugen, M. (2011). MicroRNA evolution by arm switching. EMBO. Rep. *12*, 172–177.
10. Li, S.C., Liao, Y.L., Ho, M.R., Tsai, K.W., Lai, C.H., and Lin, W.C. (2012). miRNA arm selection and isomiR distribution in gastric cancer. BMC. Genomics *13* (*Suppl 1*), S13.
11. Tsai, K.W., Leung, C.M., Lo, Y.H., Chen, T.W., Chan, W.C., Yu, S.Y., Tu, Y.T., Lam, H.C., Li, S.C., Ger, L.P., et al. (2016). Arm selection preference of microRNA-193a varies in breast cancer. Sci. Rep. *6*, 28176.
12. Huang, C.J., Nguyen, P.N., Choo, K.B., Sugii, S., Wee, K., Cheong, S.K., and Kamarul, T. (2014). Frequent co-expression of miRNA-5p and -3p species and cross-targeting in induced pluripotent stem cells. Int. J. Med. Sci. *11*, 824–833.
13. Choo, K.B., Soon, Y.L., Nguyen, P.N., Hiew, M.S., and Huang, C.J. (2014). MicroRNA-5p and -3p co-expression and cross-targeting in colon cancer cells. J. Biomed. Sci. *21*, 95.
14. Lee, D.S., Chen, J.H., Lundy, D.J., Liu, C.H., Hwang, S.M., Pabon, L., Shieh, R.C., Chen, C.C., Wu, S.N., Yan, Y.T., et al. (2015). Defined microRNAs induce aspects of maturation in mouse and human embryonic-stem-cell-derived cardiomyocytes. Cell Rep. *12*, 1960–1967.
15. Xing, Y., Liu, Z., Yang, G., Gao, D., and Niu, X. (2015). MicroRNA expression profiles in rats with selenium deficiency and the possible role of the Wnt/beta-catenin signaling pathway in cardiac dysfunction. Int. J. Mol. Med. *35*, 143–152.
16. Reddy, S., Zhao, M., Hu, D.Q., Fajardo, G., Hu, S., Ghosh, Z., Rajagopalan, V., Wu, J.C., and Bernstein, D. (2012). Dynamic microRNA expression during the transition from right ventricular hypertrophy to failure. Physiol. Genomics *44*, 562–575.
17. Vacchi-Suzzi, C., Hahne, F., Scheubel, P., Marcellin, M., Dubost, V., Westphal, M., Boeglen, C., Büchmann-Møller, S., Cheung, M.S., Cordier, A., et al. (2013). Heart structure-specific transcriptomic atlas reveals conserved microRNA-mRNA interactions. PLoS One *8*, e52442.
18. Li, Z., Song, Y., Liu, L., Hou, N., An, X., Zhan, D., Li, Y., Zhou, L., Li, P., Yu, L., et al. (2017). miR-199a impairs autophagy and induces cardiac hypertrophy through mTOR activation. Cell Death Differ. *24*, 1205–1213.
19. Li, Z., Liu, L., Hou, N., Song, Y., An, X., Zhang, Y., Yang, X., and Wang, J. (2016). miR-199-sponge transgenic mice develop physiological cardiac hypertrophy. Cardiovasc. Res. *110*, 258–267.
20. Song, X.W., Li, Q., Lin, L., Wang, X.C., Li, D.F., Wang, G.K., Ren, A.J., Wang, Y.R., Qin, Y.W., Yuan, W.J., et al. (2010). MicroRNAs are dynamically regulated in hypertrophic hearts, and miR-199a is essential for the maintenance of cell size in cardiomyocytes. J. Cell Physiol. *225*, 437–443.
21. el Azzouzi, H., Leptidis, S., Dirkx, E., Hoeks, J., van Bree, B., Brand, K., et al. (2013). The hypoxia-inducible microRNA cluster miR-199a ∼ 214 targets

myocardial PPARdelta and impairs mitochondrial fatty acid oxidation. Cell Metab. *18*, 341–354.

22. Alexander, M.S., Kawahara, G., Motohashi, N., Casar, J.C., Eisenberg, I., Myers, J.A., Gasperini, M.J., Estrella, E.A., Kho, A.T., Mitsuhashi, S., et al. (2013). MicroRNA-199a is induced in dystrophic muscle and affects WNT signaling, cell proliferation, and myogenic differentiation. Cell Death Differ. *20*, 1194–1208.
23. Haghikia, A., Missol-Kolka, E., Tsikas, D., Venturini, L., Brundiers, S., Castoldi, M., Muckenthaler, M.U., Eder, M., Stapel, B., Thum, T., et al. (2011). Signal transducer and activator of transcription 3-mediated regulation of miR-199a-5p links cardiomyocyte and endothelial cell function in the heart: a key role for ubiquitin-conjugating enzymes. Eur. Heart J. *32*, 1287–1297.
24. Gao, Y., Han, D., Sun, L., Huang, Q., Gai, G., Wu, Z., Meng, W., and Chen, X. (2018). PPARα regulates the proliferation of human glioma cells through miR-214 and E2F2. Biomed. Res. Int. *2018*, 3842753.
25. Zhang, X., Liu, L., Dou, C., Cheng, P., Liu, L., Liu, H., Ren, S., Wang, C., Jia, S., Chen, L., et al. (2019). PPAR gamma-regulated microRNA 199a-5p underlies bone marrow adiposity in aplastic anemia. Mol. Ther. Nucleic Acids *17*, 678–687.
26. Gabisonia, K., Prosdocimo, G., Aquaro, G.D., Carlucci, L., Zentilin, L., Secco, I., Ali, H., Braga, L., Gorgodze, N., Bernini, F., et al. (2019). MicroRNA therapy stimulates uncontrolled cardiac repair after myocardial infarction in pigs. Nature *569*, 418–422.
27. Lu, Z., Xu, X., Hu, X., Fassett, J., Zhu, G., Tao, Y., Li, J., Huang, Y., Zhang, P., Zhao, B., et al. (2010). PGC-1 alpha regulates expression of myocardial mitochondrial antioxidants and myocardial oxidative stress after chronic systolic overload. Antioxid. Redox Signal. *13*, 1011–1022.
28. Chen, D., Li, Z., Bao, P., Chen, M., Zhang, M., Yan, F., Xu, Y., Ji, C., Hu, X., Sanchis, D., et al. (2019). Nrf2 deficiency aggravates angiotensin II-induced cardiac injury by increasing hypertrophy and enhancing IL-6/STAT3-dependent inflammation. Biochim. Biophys. Acta Mol. Basis Dis. *1865*, 1253–1264.
29. Huang, Q., Zhou, H.J., Zhang, H., Huang, Y., Hinojosa-Kirschenbaum, F., Fan, P., Yao, L., Belardinelli, L., Tellides, G., Giordano, F.J., et al. (2015). Thioredoxin-2 inhibits mitochondrial reactive oxygen species generation and apoptosis stress kinase-1 activity to maintain cardiac function. Circulation *131*, 1082–1097.
30. Zhang, L., Chen, C.L., Kang, P.T., Jin, Z., and Chen, Y.R. (2017). Differential protein acetylation assists import of excess SOD2 into mitochondria and mediates SOD2 aggregation associated with cardiac hypertrophy in the murine SOD2-tg heart. Free Radic. Biol. Med. *108*, 595–609.
31. Nie, P., Meng, F., Zhang, J., Wei, X., and Shen, C. (2019). Astragaloside IV exerts a myocardial protective effect against cardiac hypertrophy in rats, partially via activating the Nrf2/HO-1 signaling pathway. Oxid. Med. Cell Longev. *2019*, 4625912.
32. Waldman, M., Cohen, K., Yadin, D., Nudelman, V., Gorfil, D., Laniado-Schwartzman, M., Kornwoski, R., Aravot, D., Abraham, N.G., Arad, M., et al. (2018). Regulation of diabetic cardiomyopathy by caloric restriction is mediated by intracellular signaling pathways involving 'SIRT1 and PGC-1α. Cardiovasc. Diabetol. *17*, 111.
33. Jia, D., Hou, L., Lv, Y., Xi, L., and Tian, Z. (2019). Postinfarction exercise training alleviates cardiac dysfunction and adverse remodeling via mitochondrial biogenesis and SIRT1/PGC-1α/PI3K/Akt signaling. J. Cell Physiol. *234*, 23705–23718.
34. Chen, Y., Chang, Y., Zhang, N., Guo, X., Sun, G., and Sun, Y. (2018). Atorvastatin attenuates myocardial hypertrophy in spontaneously hypertensive rats via the C/EBPβ/PGC-1α/UCP3 pathway. Cell Physiol. Biochem. *46*, 1009–1018.
35. Ahuja, P., Sdek, P., and MacLellan, W.R. (2007). Cardiac myocyte cell cycle control in development, disease, and regeneration. Physiol. Rev. *87*, 521–544.
36. Li, J.M., Pan, X.C., Ding, Y.Y., Tong, Y.F., Chen, X.H., Liu, Y., and Zhang, H.G. (2020). Effect of triptolide on temporal expression of cell cycle regulators during cardiac hypertrophy. Front. Pharmacol. *11*, 566938.
37. Hille, S., Dierck, F., Kühl, C., Sosna, J., Adam-Klages, S., Adam, D., Lüllmann-Rauch, R., Frey, N., and Kuhn, C. (2016). Dyrk1a regulates the cardiomyocyte cell cycle via D-cyclin-dependent Rb/E2f-signalling. Cardiovasc. Res. *110*, 381–394.
38. Ebelt, H., Hufnagel, N., Neuhaus, P., Neuhaus, H., Gajawada, P., Simm, A., Müller-Werdan, U., Werdan, K., and Braun, T. (2005). Divergent siblings: E2F2 and E2F4 but not E2F1 and E2F3 induce DNA synthesis in cardiomyocytes without activation of apoptosis. Circ. Res. *96*, 509–517.
39. Huang, S., Zou, X., Zhu, J.N., Fu, Y.H., Lin, Q.X., Liang, Y.Y., Deng, C.Y., Kuang, S.J., Zhang, M.Z., Liao, Y.L., et al. (2015). Attenuation of microRNA-16 derepresses the cyclins D1, D2 and E1 to provoke cardiomyocyte hypertrophy. J. Cell Mol. Med. *19*, 608–619.
40. Dobaczewski, M., Chen, W., and Frangogiannis, N.G. (2011). Transforming growth factor (TGF)-β signaling in cardiac remodeling. J. Mol. Cell Cardiol. *51*, 600–606.
41. Hu, H.H., Chen, D.Q., Wang, Y.N., Feng, Y.L., Cao, G., Vaziri, N.D., and Zhao, Y.Y. (2018). New insights into TGF-β/Smad signaling in tissue fibrosis. Chem. Biol. Interact. *292*, 76–83.
42. Bugyei-Twum, A., Ford, C., Civitarese, R., Seegobin, J., Advani, S.L., Desjardins, J.F., Kabir, G., Zhang, Y., Mitchell, M., Switzer, J., et al. (2018). Sirtuin 1 activation attenuates cardiac fibrosis in a rodent pressure overload model by modifying Smad2/3 transactivation. Cardiovasc. Res. *114*, 1629–1641.
43. Cappetta, D., Esposito, G., Piegari, E., Russo, R., Ciuffreda, L.P., Rivellino, A., Berrino, L., Rossi, F., De Angelis, A., and Urbanek, K. (2016). SIRT1 activation attenuates diastolic dysfunction by reducing cardiac fibrosis in a model of anthracycline cardiomyopathy. Int. J. Cardiol. *205*, 99–110.
44. Rane, S., He, M., Sayed, D., Vashistha, H., Malhotra, A., Sadoshima, J., Vatner, D.E., Vatner, S.F., and Abdellatif, M. (2009). Downregulation of miR-199a derepresses hypoxia-inducible factor-1alpha and sirtuin 1 and recapitulates hypoxia preconditioning in cardiac myocytes. Circ. Res. *104*, 879–886.
45. Oka, S., Alcendor, R., Zhai, P., Park, J.Y., Shao, D., Cho, J., Yamamoto, T., Tian, B., and Sadoshima, J. (2011). PPARα-Sirt1 complex mediates cardiac hypertrophy and failure through suppression of the ERR transcriptional pathway. Cell Metab. *14*, 598–611.
46. Li, S., Zhu, Z., Xue, M., Yi, X., Liang, J., Niu, C., Chen, G., Shen, Y., Zhang, H., Zheng, J., et al. (2019). Fibroblast growth factor 21 protects the heart from angiotensin II-induced cardiac hypertrophy and dysfunction via SIRT1. Biochim. Biophys. Acta Mol. Basis Dis. *1865*, 1241–1252.
47. Ma, S., Feng, J., Zhang, R., Chen, J., Han, D., Li, X., Yang, B., Li, X., Fan, M., Li, C., et al. (2017). SIRT1 activation by resveratrol alleviates cardiac dysfunction via mitochondrial regulation in diabetic cardiomyopathy mice. Oxid. Med. Cell Longev. *2017*, 4602715.
48. Lin, E.A., Kong, L., Bai, X.H., Luan, Y., and Liu, C.J. (2009). miR-199a, a bone morphogenic protein 2-responsive MicroRNA, regulates chondrogenesis via direct targeting to Smad1. J. Biol. Chem. *284*, 11326–11335.
49. Qu, F., Zheng, J., Gan, W., Lian, H., He, H., Li, W., Yuan, T., Yang, Y., Li, X., Ji, C., et al. (2017). MiR-199a-3p suppresses proliferation and invasion of prostate cancer cells by targeting Smad1. Oncotarget *8*, 52465–52473.
50. Hanna, A., Humeres, C., and Frangogiannis, N.G. (2021). The role of Smad signaling cascades in cardiac fibrosis. Cell Signal. *77*, 109826.
51. Yang, Z., Xiao, Z., Guo, H., Fang, X., Liang, J., Zhu, J., Yang, J., Li, H., Pan, R., Yuan, S., et al. (2019). Novel role of the clustered miR-23b-3p and miR-27b-3p in enhanced expression of fibrosis-associated genes by targeting TGFBR3 in atrial fibroblasts. J. Cell Mol. Med. *23*, 3246–3256.
52. Chen, X., Xu, J., Jiang, B., and Liu, D. (2016). Bone morphogenetic protein-7 antagonizes myocardial fibrosis induced by atrial fibrillation by restraining transforming growth factor-β (TGF-β)/Smads signaling. Med. Sci. Monit. *22*, 3457–3468.
53. Morine, K.J., Qiao, X., York, S., Natov, P.S., Paruchuri, V., Zhang, Y., Aronovitz, M.J., Karas, R.H., and Kapur, N.K. (2018). Bone morphogenetic protein 9 reduces cardiac fibrosis and improves cardiac function in heart failure. Circulation *138*, 513–526.
54. Turner, N.A. (2011). Therapeutic regulation of cardiac fibroblast function: targeting stress-activated protein kinase pathways. Future Cardiol. *7*, 673–691.
55. Eulalio, A., Mano, M., Dal Ferro, M., Zentilin, L., Sinagra, G., Zacchigna, S., and Giacca, M. (2012). Functional screening identifies miRNAs inducing cardiac regeneration. Nature *492*, 376–381.

56. Tang, C.M., Liu, F.Z., Zhu, J.N., Fu, Y.H., Lin, Q.X., Deng, C.Y., Hu, Z.Q., Yang, H., Zheng, X.L., Cheng, J.D., et al. (2016). Myocyte-specific enhancer factor 2C: a novel target gene of miR-214-3p in suppressing angiotensin II-induced cardiomyocyte hypertrophy. Sci. Rep. *6*, 36146.

57. Liang, J.N., Zou, X., Fang, X.H., Xu, J.D., Xiao, Z., Zhu, J.N., Li, H., Yang, J., Zeng, N., Yuan, S.J., et al. (2019). The Smad3-miR-29b/miR-29c axis mediates the protective effect of macrophage migration inhibitory factor against cardiac fibrosis. Biochim. Biophys. Acta Mol. Basis Dis. *1865*, 2441–2450.

58. Yuan, W., Tang, C., Zhu, W., Zhu, J., Lin, Q., Fu, Y., Deng, C., Xue, Y., Yang, M., Wu, S., et al. (2016). CDK6 mediates the effect of attenuation of miR-1 on provoking cardiomyocyte hypertrophy. Mol. Cell Biochem. *412*, 289–296.

59. Orom, U.A., and Lund, A.H. (2007). Isolation of microRNA targets using biotinylated synthetic microRNAs. Methods *43*, 162–165.

60. Baylin, S.B., and Schuebel, K.E. (2007). Genomic biology: the epigenomic era opens. Nature *448*, 548–549.